Journal of Power Sources 353 (2017) 183–194

Contents lists available at ScienceDirect

Journal of Power Sources

journal homepage: www.elsevier.com/locate/jpowsour

Impedance change and capacity fade of lithium nickel manganese cobalt oxide-based batteries during calendar aging

Julius Schmitt [a], Arpit Maheshwari [a, b], Michael Heck [a, *], Stephan Lux [a], Matthias Vetter [a]

[a] Fraunhofer Institute for Solar Energy Systems, Heidenhofstraße 2, 79110, Freiburg, Germany
[b] Politecnico di Torino, Corso Duca degli Abruzzi 24, 10129, Turin, Italy

HIGHLIGHTS

- Calendar aging tests on lithium-ion batteries at different storage conditions.
- Analysis of changes in cell impedance via current pulse tests and EIS.
- Quantitative description of cell impedance by equivalent circuit parameters.
- Observation of significant influence of electrochemical characterization on aging.

ARTICLE INFO

Article history:
Received 17 November 2016
Received in revised form
1 February 2017
Accepted 21 March 2017
Available online 8 April 2017

Keywords:
Lithium-ion battery
Calendar aging
Capacity fade
Cell impedance
Lifetime prediction
Electrochemical impedance spectroscopy

ABSTRACT

The calendar aging of commercial 18650 lithium-ion batteries with lithium nickel manganese cobalt oxide cathode and graphite anode is studied by regular electrochemical characterization of batteries stored at defined conditions. The cell capacity is found to decrease linearly with time and shows a faster decrease at higher storage temperatures. From current pulse tests, it is determined that both higher temperature and higher state of charge (SOC) cause accelerated resistance increase with storage time. Changes in different battery parameters during storage are also quantified by analyzing electrochemical impedance spectroscopy (EIS) spectra. The cell degradation causes a gradual increase of the ohmic and the total polarization resistance with storage duration, where the latter one is found to be the main contributor to the increased cell impedance. An increase in the mean relaxation time constant and changes in the porous structure for the electrode processes are observed from EIS analysis. Resistance for this cell chemistry is found to be current independent by comparing the cell resistance calculated from the current pulse method after 1s and from the EIS analysis at 1 Hz. Furthermore, it is seen that the additional charge throughput due to the periodic electrochemical characterization induces significant cell degradation effects.

1. Introduction

Lithium-ion batteries are nowadays the preferred energy storage technology for portable applications such as consumer electronics, power tools and electrified vehicles because of their high volumetric and gravimetric energy density. Due to decreasing prices, they are also becoming an interesting technology for stationary energy storage. The requirements and expectations on the lifetime of battery packs for electric vehicles and stationary energy storage systems are usually much higher than for consumer products, especially because the cost of the battery pack represents a significant share of the cost of the whole product. Reliable forecasts on the battery lifetime at certain operating conditions are thus essential in order to minimize financial risks for stakeholders in the battery industry.

The most important aging effects occurring in lithium-ion batteries are cell capacity fade and power fade. These effects haven been intensively studied by many groups [1–8]. The capacity fade and power fade depend on time, charge throughput and the operating parameters: temperature, state of charge (SOC), current amplitude and depth of discharge (DOD).

It is a common approach to distinguish between calendar and cycle aging of lithium-ion batteries [4,5,7,9]. Calendar aging describes the cell degradation during storage, i.e. without applying a

* Corresponding author.
E-mail address: michael.heck@ise.fraunhofer.de (M. Heck).

http://dx.doi.org/10.1016/j.jpowsour.2017.03.090
0378-7753/

current to the cell, while cycle aging describes the cell degradation which occurs during charging and discharging of batteries. This differentiation is based on the assumption that there are aging mechanisms which occur independently of whether the cell is cycled (calendar aging) and additional mechanisms which only arise if the cell is operated (cycle aging).

The calendar aging is usually investigated by alternating storage periods and electrochemical characterizations. The exact method is not standardized and depends on the desired application and the type of lithium-ion battery. The storage duration interval between the electrochemical characterization is found to vary from 20 days [10], 42 days [4,11], 49 days [12], 60 days [3], 90 days up to 2–9 month [8]. Also the procedure for electrochemical characterization for determination of the actual cell capacity, the internal resistance and EIS measurement is different for each aging experiment. In the articles [3,8,10,12], the influence of additional charge throughput from characterization on the capacity fade and the impedance rise was not mentioned. The calendar aging tests can also be conducted either at open circuit conditions or at constant voltage conditions [4,11,12].

Many authors regard the loss of active lithium as the dominant mechanism causing capacity fade [5,7,8,13,14]. This is based on the assumption that the degradation of both the cathode and anode are much slower than the consumption of available active lithium. Thus, the lithium inventory is the capacity limiting factor. Active lithium is mostly lost through electrolyte reduction at the anode surface which leads to the formation of an insulating solid electrolyte interphase (SEI) adjacent to the anode surface [15,16].

The SEI is initially built during cell formation but keeps on growing at a much slower rate afterwards [16,17]. Different theories for the processes that limit the rate of SEI growth have been discussed. Some authors describe an electron current through the SEI as rate limiting factor which can be described by electron diffusion, migration or tunneling [3,15,18]. Ploehn et al. [2] described the process as being limited by the diffusion of reactive solvent molecules through the SEI which are then reduced at the SEI/graphite interface. All of these theories suggest a continuous decrease of the SEI growth rate due to the increase of SEI thickness. The capacity fade during calendar aging is thus often described by a square root of time dependence [9,15,19].

Other authors use different model functions to describe the calendar capacity fade. Chirstensen et al. [16] assume the capacity to decrease linearly with time at the beginning and with square root of time at a later stage. Belt et al. [20] found a linear capacity decrease with time for cells stored between 30 °C and 50 °C and a square root of time decrease with time for cells stored at 60 °C. Schmalstieg et al. [21] discussed a superposition of linear and square root dependence and used a power law function to achieve a consistent description of this behavior. Baghdadi et al. [22] described the calendar capacity fade by an exponential function.

Besides capacity fade, changes in the cell impedance during calendar aging of lithium-ion batteries have been discussed in the literature [4,8,9,12,20,23]. In most cases, an increase of the overall internal resistance is found, which is attributed to the growth of surface films on both electrodes.

Electrochemical impedance spectroscopy (EIS) remains one of the most successful non-destructive characterization techniques for delving deeper into understanding the individual processes and process changes of an electrochemical cell. This technique has been used for characterization of batteries usually to ascertain dependence of the spectra on SOC and temperature [24,25]. However, not many studies that analyze battery aging using EIS spectra are available. Moreover, when available, this analysis is usually qualitative and at best only a part of the information rich spectra is quantified [17,26–28]. Fitting of EIS data with an equivalent circuit model to quantify aging is seen only in some works [6,10,29,30], while in other literature on battery aging [4,5,12], EIS tests were performed but no EIS analysis results were presented by the authors.

Degradation mechanisms, such as loss of active mass and loss of active lithium, affect the open circuit voltage (OCV) of lithium ion cells [31,32], which can even be used to study degradation. However, the effect of storage time on OCV has not been studied. In this work, the changes of both cell capacity and cell impedance during calendar aging are studied using commercial 18650 lithium-ion cells. The description of changes in cell impedance is based on pulse test measurements and an in-depth electrochemical impedance spectra analysis. For this analysis, an in-house code was developed to de-convolute EIS spectra using an equivalent circuit model. Calendar aging of the cells was then studied by quantifying the change in the different parameters of the model and associating them with degradation mechanisms leading to changes of the electrochemical behavior. Additionally, the evolution of internal resistance resulting from pulse test and the total resistance from EIS analysis are compared.

Furthermore, from the analysis of reference cells, characterization procedure and EIS, it is shown that the regular electrochemical characterizations carried out during the calendar aging tests significantly influences the determined capacity fade, impedance rise and change of EIS spectra. The additional charge throughput from periodic electrochemical characterizations causes cell degradation over and above the calendar aging. This has been qualitatively discussed in the text.

2. Experimental

2.1. Tested batteries

Commercial 18650 high energy cylindric cells of the type US18650V3 manufactured by Sony Energy Devices Corporation were tested. Their cathode active material is lithium nickel manganese cobalt oxide (NMC) and the anode active material is graphite. The rated capacity according to the manufacturer is 2.15 Ah measured at a discharge current rate of 0.2 C. This capacity value is used as reference for calculating current rates (C-rates).

2.2. Battery test system

All aging tests were done with a BaSyTec CTS Battery Test System from BaSyTec GmbH. Electrochemical impedance spectroscopy was conducted with a Digatron EIS-Meter 2-20-2 from Digatron Industrie-Elektronik GmbH.

2.3. Calendar aging tests

During the calendar aging tests, the cells were stored under controlled conditions in climatic chambers. After a storage duration of approximately 30 days, the cells were placed in the temperature chamber at 20 °C until they reached their thermodynamical equilibrium. Then, the electrochemical characterization was conducted followed by resetting the SOC.

2.4. Characterization

The characterizations and setting of SOC were conducted at an ambient temperature of 20 °C. The batteries were first fully charged using constant current charging up to 4.2 V at a current rate of 1 C followed by constant voltage charging until the current had decreased to 0.05 C (CCCV charging). Then, two cycles consisting of constant current discharging to 2.5 V at 1 C (CC discharging) and

CCCV charging were conducted. The discharge capacity during the second cycle was regarded as actual cell capacity C_{1C}.

Afterwards, the cells were CC discharged and CCCV charged with a current rate of 0.1 C. The charge withdrawn during this discharging step is denoted as actual cell capacity $C_{0.1C}$ which is used for analyzing the capacity decrease (see section 3.1).

The cell impedance was subsequently tested by applying 2 C discharging pulses of 20 s duration followed by 1 C charging pulses of 40 s duration. The pulses were applied at each 10 % SOC between 100 % and 0 % SOC. The SOC levels were set by 1 C discharging 10 % of the capacity C_{1C} followed by a pause of 30 min.

Then the cells were CCCV charged with a current rate of 1 C and afterwards set to 50 % SOC by CC discharging of 0.5 C_{1C}.

Subsequently, EIS measurements were done in galvanostatic mode in the frequency range of 2 kHz–10 mHz with 8 points of measurement per decade. Measurements were conducted at open circuit voltage (no applied direct current), the ideal voltage response was set to 10 mV and the maximum AC amplitude was set to 0.2 A.

2.5. Storage

The combinations of tested temperatures and SOC during storage is shown in Table 1. In order to see statistical effects, each test was performed with three cells. After the characterization procedure, the cells were set to a defined SOC. Since the characterization ends at 50 % SOC, no SOC correction was needed for cells stored at this SOC at the three temperatures. For the storage conditions at 100 % SOC, the cells were fully charged using CCCV charging at 1 C. For setting other storage SOC levels, the cells were CCCV charged and subsequently CC discharged with 1 C. They were then CCCV charged and the corresponding part of the charge extracted during the preceding discharging step was withdrawn using CC discharging at 1 C to set the SOC. Afterwards, the cells were disconnected from the battery test system and stored at defined ambient temperatures T for approximately 30 days. The results shown in this work are based on approximately 470 days of observed aging (approximately 360 days for EIS analysis).

2.6. Reference cells

In order to study the influence of the characterization procedure on cell degradation, four cells were used as reference. They were initially characterized and set to 25 %, 50 %, 75 % and 100 % storage SOC by the same procedure as the other cells. Afterwards, they were kept at open circuit conditions at 20 °C. The cells' open-circuit voltage was checked every 30 days in order to monitor self-discharging. If the open-circuit voltage was found to be lower than directly after the initial setting of the SOC, the cell was CCCV charged to the initial open-circuit voltage in order to compensate self-discharging. The amount of charge transferred during these procedures was found to be very small in comparison with cell capacity. Self-discharging is therefore negligible for the tested cells during the tested time intervals. Besides these controls, the reference cells were stored without any further characterization until they were finally characterized after 186 days.

Table 1
Test matrix of studied storage conditions. Tested combinations of SOC and ambient temperature are marked by an 'x'.

SOC	$T = 0$ °C	$T = 20$ °C	$T = 45$ °C
25 %		x	
50 %	x	x	x
75 %		x	
100 %	x	x	x

3. Results and discussion

3.1. Cell capacity

3.1.1. Time dependency

The actual cell capacity determined at 0.1 C discharging $C^{act}_{0.1C}$ relative to the initial capacity $C^{ini}_{0.1C}$ is plotted versus storage time in Fig. 1. Each data point corresponds to the arithmetic mean of the actual relative capacity of three cells tested under the same conditions, which always have very similar values. The mean initial cell capacity is 2.164 Ah with a standard deviation of 0.006 Ah, which is a sign of high homogeneity between the samples.

The cell capacity decreases with storage time for all tested cells. This capacity fade can be assigned to the loss of active lithium [5,7,8,13,14]. In order to understand the capacity fade as a function of time three model functions (square root, linear and generalized power function) are fitted to the data. As discussed in section 1, many authors describe the capacity fade during calendar aging as a square root of time function based on the assumption that the growth of the SEI slows down the further consumption of active lithium [5,9,15]. This behavior is modeled by Eq. (1) where a_1 and a_2 are offset and square root aging parameter, respectively and t the storage time in days:

$$C^{act}(t) \Big/ C^{ini} = a_1 - a_2 \cdot \sqrt{t}. \quad (1)$$

The linear capacity fade with time, as observed in the work of [20], with b_1 and b_2 as offset and linear aging parameter, respectively is given by Eq. (2):

$$C^{act}(t) \Big/ C^{ini} = b_1 - b_2 \cdot t. \quad (2)$$

The third tested model function is a generalized power law function with offset c_1, power aging parameter c_2 and the exponent c_3:

$$C^{act}(t) \Big/ C^{ini} = c_1 - c_2 \cdot t^{c_3}. \quad (3)$$

For the offset parameters a_1, b_1 and c_1, values near 1 are expected, as all three model functions refer to the relative capacity.

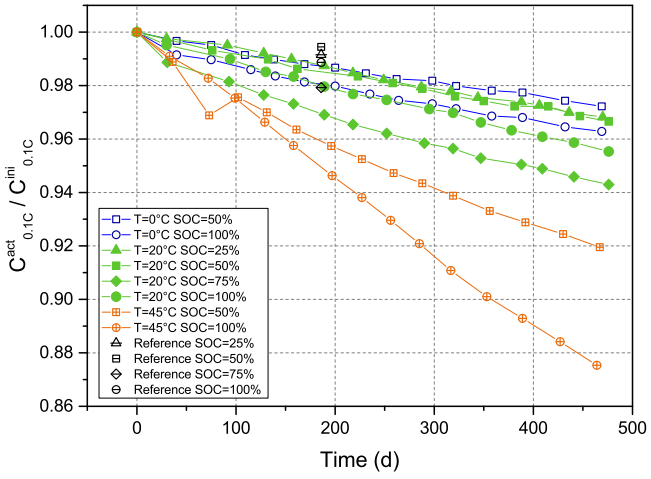

Fig. 1. Relative cell capacity during calendar aging tests plotted versus storage time for various storage temperatures and storage SOC. Additionally, the relative cell capacity of the reference cells, which were stored for 186 days at 20 °C with no intermediate characterizations, is displayed.

Linear regression was used to fit the square root of time function and the linear function to the experimental data shown in Fig. 1. For fitting the power law function, nonlinear fitting using the Levenberg-Marquardt algorithm was applied. The estimated parameters of the three model functions are tabulated in Table 2.

For most data sets, the coefficient of determination R^2 is larger for the linear model function than for the square root of time function. This means that the fit accuracy is higher for the linear model function. Fitting the power law function to the data yields even higher R^2-values for most data sets. The reason is that the power law function has one fitting parameter more than the linear model, which is the exponent c_3. The estimated exponents c_3 show significant variance as they are in the range $0.72 - 0.96$ (see Table 2). It can be noted that the values are closer to 1 (linear) than to 0.5 (square root) but show no trend of variation. An explanation for this behavior could be that besides the constant growth of SEI other degradation mechanisms that do not slow down during prolonged storage could cause a linear part of the capacity decrease. Such "in between" functionality is also found in the literature [21]. It is possible that the observed capacity fade is a superposition of capacity loss due to SEI growth at open circuit conditions which follows square root of time dependency and additional capacity fade caused by charging and discharging the cells during characterizations, as will be discussed in more detail in section 3.3.

For this work, in order to ascertain the influence of the operating parameters (T, storage SOC) on capacity fade, the linear aging parameter b_2 is chosen. An important point to remember here is that a linear model is chosen for further analysis because of its simplicity and because it fits the capacity decrease satisfactorily.

3.1.2. Temperature dependency

The temperature dependency of the capacity fade shows a clear trend. At 50 % storage SOC, the rate of capacity fade b_2 is slightly higher at 20 °C compared to 0 °C (see Table 2). The rate of capacity decrease at 45 °C is more than twice the rate at 20 °C. A similar trend is observed at 100 % storage SOC.

An approach to model the temperature dependency of capacity fade during calendar aging is the Arrhenius equation [4,9,22,33].

$$k = A \cdot \exp\left(-\frac{E_a}{R \cdot T}\right) \quad (4)$$

where k is the reaction rate, A a pre-exponential factor, E_a the activation energy, R the gas constant and T the absolute temperature. Table 3 shows the parameters of the Arrhenius equation extracted from regression to the capacity fade rates b_2 at different temperatures for two different storage SOC. The coefficient of determination R^2 is above 0.9, indicating that the temperature dependency of the capacity fade rate can be appropriately described by the Arrhenius equation. The obtained values for the activation energy are in the same order of magnitude as found by other authors [1,4].

Table 3
Fitted parameter values of the Arrhenius equation describing the influence of storage temperature on the rate of capacity fade with time at two storage SOC levels.

SOC (%)	A (d^{-1})	E_a (J mol^{-1})	R^2
50	0.35	2.04E+04	0.94
100	9.82	2.78E+04	0.96

A physical interpretation of this temperature behavior is increased electronic conductivity of the SEI at elevated temperatures, which leads to a higher electronic current across this layer and finally results in a higher rate of electrolyte decomposition at the SEI/electrolyte interface.

3.1.3. SOC dependency

The rate of capacity decrease is significantly higher for cells stored at 100 % SOC compared to cells stored at 50 % SOC at all tested temperatures as illustrated in Fig. 1. Accelerated capacity fade at high SOC was found by many authors [1,4,7,8,12,21]. For example Keil et al. [8] showed that low graphite anode potentials at high SOC facilitate electrolyte reduction and SEI growth and thus lead to accelerated loss of active lithium during calendar aging. The cells stored at 25 % SOC and 75 % SOC at 20 °C do not follow this trend. The 25 % SOC cells lose their capacity slightly faster than the cells stored at 50 % SOC. The cells stored at 75 % SOC show the fastest capacity decrease of all tested SOC levels. This behavior might be due to the experimental procedure of resetting the SOC after the characterization as will be discussed in Section 3.3.

3.2. Cell impedance

The cell impedance is studied via current pulse measurements and EIS. Current pulses allow the determination of an overall resistance at a certain SOC, temperature and current magnitude. EIS is only conducted at open circuit voltage (OCV) but gives more detailed information than pulse tests about changes in electrochemical phenomena inside the cell.

3.2.1. Pulse tests

The internal resistance of a cell R (defined for a particular SOC of the battery) is derived from the overvoltage due to a current pulse with current amplitude I, i. e. $R = (U_{OCV} - U_t)/I$ where U_{OCV} is the equilibrium voltage before the pulse and U_t the terminal voltage after a certain time. It is assumed that the current pulse does not change the SOC significantly so that the open circuit voltage does not change during the pulse duration. For simplicity, only the internal resistance measured at 50 % SOC is discussed here, because a similar trend is found at other SOC points.

Fig. 2(a) shows the internal resistance, R_{1s}, based on the voltage

Table 2
Fitted parameter values for model functions describing the capacity decrease due to calendar aging. Dimensionless parameter values are tabulated.

T (°C)	SOC (%)	sqrt.			linear			power			
		a_1	a_2	R^2	b_1	b_2	R^2	c_1	c_2	c_3	R^2
0	50	1.005	1.36E-03	0.952	0.999	5.71E-05	0.991	1.001	2.42E-04	0.77	0.996
0	100	1.003	1.78E-03	0.980	0.995	7.28E-05	0.976	0.997	2.75E-04	0.79	0.997
20	25	1.007	1.62E-03	0.916	1.000	6.94E-05	0.996	1.001	9.05E-05	0.96	0.995
20	50	1.005	1.60E-03	0.939	0.999	6.78E-05	0.993	1.000	1.44E-04	0.88	0.994
20	75	1.004	2.70E-03	0.984	0.992	1.10E-04	0.972	0.997	6.22E-04	0.72	0.998
20	100	1.007	2.16E-03	0.946	0.998	9.09E-05	0.996	0.999	1.53E-04	0.92	0.998
45	50	1.009	3.89E-03	0.963	0.991	1.60E-04	0.969	0.996	6.06E-04	0.79	0.980
45	100	1.027	6.42E-03	0.920	1.001	2.77E-04	0.999	1.004	3.83E-04	0.95	0.999

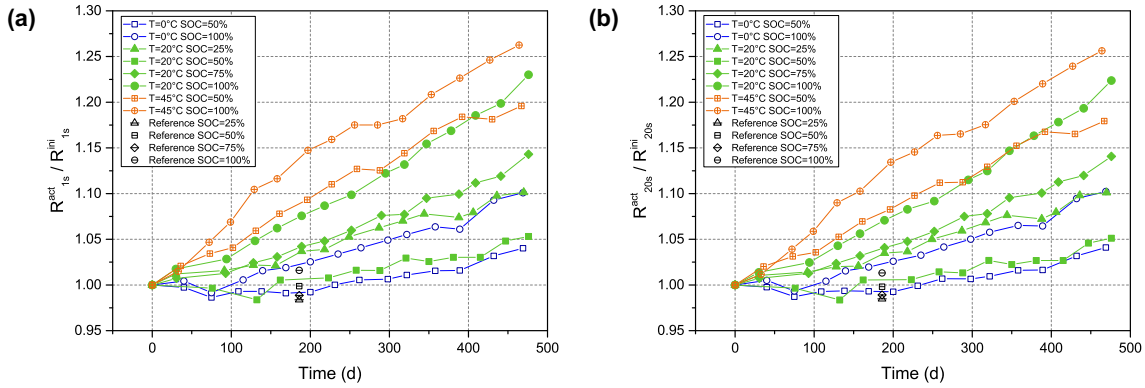

Fig. 2. Internal resistance determined by current pulse tests measured at 50 % SOC plotted versus storage time. Storage conditions are indicated in the legend. Besides the results from the calendar aging tests, the internal resistance of the reference cells, which were stored for 186 days at 20 °C with no intermediate characterizations, is displayed. (a) Internal resistance calculated from the voltage drop after 1 s of discharging the cells with a current rate of 2 C. (b) Internal resistance calculated from the voltage drop after 20 s of discharging the cells with a current rate of 2 C.

response measured after 1 s of the current pulse as a function of storage time. This quantity signifies the overall resistance due to effects which do not include impedance effects due to diffusion processes.

The change of internal resistance in Fig. 2(a) can approximately be described as a linear function of time. Increase of internal resistance during calendar aging is often explained with increased ionic resistance due to the formation of surface layers (e. g. SEI) [15,21]. The rate of resistance increase is significantly higher for cells stored at 45 °C compared to cells stored at lower temperatures. In addition, a general trend of faster resistance increase for cells stored at higher SOC can be observed from Fig. 2(a). In particular, the resistance increases significantly faster for cells stored at 100 % SOC than for cells stored at 50 % SOC at the same temperature.

Exceptionally to this trend, the internal resistance for cells stored at 20 °C with 50 % SOC and for cells stored at 0 °C with 50 % SOC initially decreases and only starts increasing after about 200 days while the actual capacity continuously decreases (see Fig. 1). Käbitz et al. [4] proposed that cycling can lead to increased anode porosity resulting in a decrease of internal resistance. It might be possible that at mild storage conditions, initial resistance decrease due to cycle aging effects introduced by the electrochemical characterizations is stronger than resistance increase due to calendar aging. This results in an overall resistance decrease (see Section 3.3).

Fig. 2(b) shows the internal resistance based on the voltage response after discharging the cells for 20 s with a current rate of 2 C (R_{20s}). This quantity is a measure for the overall cell resistance including slow processes like solid state diffusion. The choice of the time durations, 20 s and 1 s, has been deliberately made in order to study resistances with and without the inclusion of solid state diffusion, respectively. The reason for this choice becomes clearer from the electrochemical impedance spectra analysis presented in the next section (Section 3.2). The relative change of R_{20s} with storage time is almost identical to the relative change observed for R_{1s}. In fact, the ratio between the two quantities R_{1s}/R_{20s} is between 75 % and 77 % for all operating conditions and during all aging stages. This means that the aging affects fast processes such as ohmic resistance and charge transfer resistance in the same way as diffusion processes.

3.2.2. Electrochemical impedance spectroscopy

EIS analysis presented in this work is carried out for a period of about 360 days starting with fresh cells. The initial impedance spectra show very little variation among the different cells, indicating good cell quality. EIS spectra of a cell stored at 45 °C and 100 % SOC at the initial measurement and at the end of the analysis period are shown in Fig. 3(a). The range of frequencies chosen for the experiments covers all crucial phenomena inside a battery. At very high frequencies (> 840 Hz), inductive effects arising from cell winding, geometry and cables are observed [34]. At the intercept of the impedance with the real axis the imaginary part of the impedance cancels out. The resulting real part is mainly due to the electrolyte's ohmic resistance [26]. In the range from 840 Hz to 1 Hz, the SEI and charge transfer at the electrodes dominate the cell impedance which takes the shape of a (depressed) semicircle in the Nyquist plot. This arises from the characteristics of both resistance and capacitance [35,36]. The depression of the semicircle is due to the porous nature of the electrodes. At low frequencies (< 1 Hz), solid state diffusion processes become important. As seen in Fig. 3(a), the impedance has the shape of a sloped line, as can be expected for diffusion processes [24]. The impedance of the calendar aged cell shows a similar nature, though it is shifted in the Nyquist plot.

The measured spectra were fitted to the equivalent circuit shown in Fig. 3(b). The cell impedance of the equivalent circuit shown in Fig. 3(b) is given by a sum of the various elements:

$$Z(\omega) = \mathrm{i}\omega L + R_s + \frac{R_p}{1 + R_p \cdot Q_p(\mathrm{i}\omega)^{\alpha}} + \frac{1}{Q_d(\mathrm{i}\omega)^{\beta}}. \quad (5)$$

This circuit employs elements for all phenomena discussed before. Fitting of spectra using an equivalent circuit model has to be carried out keeping in mind that a complex model can lead to overfitting, as is apparently seen in the work of Tröltzsch et al. [30] who fit their spectra with 13 parameters. In our case this is especially relevant in the frequency range of 840 Hz–1 Hz where only one depressed semicircle is seen (Fig. 3(a)) instead of the expected two loops representing the charge transfer and the surface layer at both electrodes. The reason is that the individual effects are superimposed in the spectra and cannot be separated using the equivalent circuit model approach. In order to study the combined effect of the polarization resistances and capacitance effects of the two electrodes, this depressed semicircle, is represented by one ZARC element. A ZARC element consists of a resistance and a constant phase element (CPE) in parallel [24]. The resistance R_p of this ZARC element represents the total polarization resistance which is the combined resistance due to charge transfer in the two electrodes and the SEI layer on the anode, while the constant phase element (Q_p) represents the sum of double layer capacitances

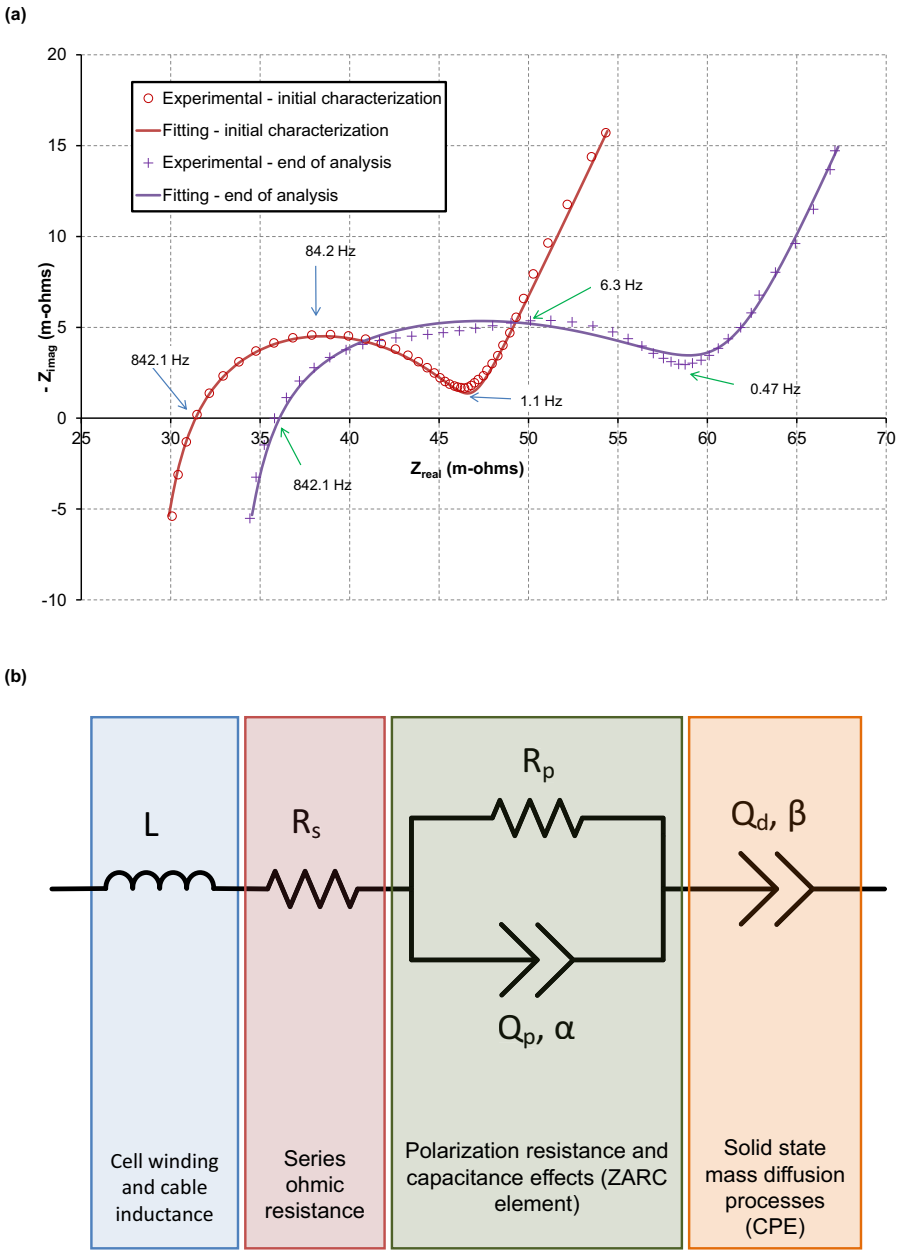

Fig. 3. (a) Nyquist plots of electrochemical impedance spectra at beginning of analysis and end of analysis period. (b) Equivalent circuit model used for fitting EIS spectra.

distributed over the porous electrode as well as resistive behavior [10,24,37,38].

The frequency dispersion is related to the CPE with the generalized polarization capacitance Q_p which has the unit $(s^{\alpha} \cdot \Omega^{-1})$. The depression factor α is a measure for the distribution of the time constants due to the porous structure of the electrode [24,37] associated with polarization processes and can take values between 0 (for a purely resistive Q_p) and 1 (for a purely capacitive Q_p). The mean time constant for polarization processes can be defined as $\tau = (R_p \cdot Q_p)^{1/\alpha}$ which has units of (s) and allows a more intuitive physical interpretation. With this substitution, the impedance is given by:

$$Z(\omega) = \mathrm{i}\omega L + R_s + \frac{R_p}{1 + (\mathrm{i}\omega\tau)^{\alpha}} + \frac{1}{Q_d(\mathrm{i}\omega)^{\beta}}. \quad (6)$$

This model contains seven fitting parameters, out of which the four R_s, R_p, α and τ are analyzed and quantified in this work. The inductance L, which is partially due to external influences such as connecting cables, has no significant importance to cell performance and aging. It is used as a fitting parameter for the very high frequency part of the curve. Analysis of the slow diffusion processes in the impedance spectra is not carried out in this work due to the difficulty of physically interpreting the CPE element. From the fitting analysis, a large scattering of the diffusion parameters Q_d and β is noticed. The reason is that no bounds on the fitting of these parameters were set due to not having any literature background defining them. The only important aspect worth mentioning is that a generalized CPE element for diffusion is chosen and not a Warburg element (with $\beta = 0.5$) because the assumption of semi-infinite diffusion [24] is not valid in our case [39,40]. Throughout the analysis period of about one year, β hovers around a value of 0.7 ($\pm$0.07) .

New cells are expected to have a small SEI resistance and thus the semicircle seen in the initial spectrum in Fig. 3(a) should be primarily due to the charge transfer resistance of the two electrodes. Though the spectrum of the aged cell in Fig. 3(a) shows a incomplete separation into (at least) two semicircles, the spectrum is still fit well enough by the chosen equivalent circuit model. The fitting parameters obtained in such cases will represent the total polarization resistances and capacitances.

In order to fit the EIS data resulting from the initial characterization to the last one after 360 days in chronological order, an in-house code that can fit the EIS spectra with the model given in Eq. (6) was developed in Octave [41]. The Levenberg-Marquardt nonlinear algorithm is used to solve least squares curve fitting. For the first data set the parameters are guessed. The resulting parameters from the least squares fit are the initial parameters for the next impedance data set. Due to individual differences of the cells, the resulting parameters of the initial fit might vary a little. Thus, the parameters are normalized to the values extracted from the fit to the spectra measured at the beginning of the experiments. Like in the analysis of the pulse tests, the average of the parameters of the three cells that are similarly aged is presented in the following. In addition, the mean absolute values for the parameters extracted from the spectra of the unaged cells are tabulated in Table 4 along with the initial inner resistances determined from pulse tests for comparison.

EIS data for about 360 days of storage has been analyzed. Notice that the limit of one year is imposed due to the increasing error of fitting obtained for the spectra fitted for aged cells, as the model function starts to show insufficiency in representing the spectrum that is seen.

3.2.3. Fitting results

The general trend of the series resistance R_s (Fig. 4(a) and (b)) is an increase during aging under all conditions of temperature and SOC. This is consistent with Waag et al. [26] and Stianzny et al. [10]. Although results from the former cannot be directly compared with ours, as their cells have the combined effect of cycle and calendar aging. From Fig. 4(a) and (b), two effects can be concluded. The series resistance increases stronger with higher temperature and the growth rate of R_s is higher for cells stored at 100 % SOC compared to 50 % SOC. The nature of the increase is quite regular in all cases. The series resistance R_s is a measure of the ohmic resistance in the cell, predominantly caused due to the conduction of lithium ions in the electrolyte [6,42]. Thus an increase in R_s points to a degradation reaction of the electrolyte, which is faster at higher voltages and thus higher SOC, as well as at higher temperatures. This irreversible reaction of electrolyte with lithium contributes to cell degradation not only by an increased resistance of the electrolyte (measured by increase in R_s), but also in loss of active lithium (see section 3.1) and formation of SEI (estimated by change in R_p).

The parallel resistance R_p, representing the polarization resistance, shows a general upward trend (Fig. 4(c) and (d)) for all cases except the batteries stored at 0 °C, 50 % SOC. In cases of high temperature and high storage SOC (45 °C, 50 % and 100 % SOC; 20 °C, 100 % SOC), the upward trend is unambiguous and demonstrates that both temperature and SOC affect this parameter. The relative change is much higher for R_p than for R_s. However for other cases, fluctuations are seen in the fitting results. The overall trend from Fig. 4(c) and (d) is that at 0 °C, very little increase in R_p is seen, while the increase at 100 % SOC is more than the increase at 50 % SOC.

Table 4
Mean initial values and standard deviation of inner cell resistance calculated from pulse tests and quantities extracted from EIS analysis.

Quantity	Initial value
R_{1s}	46.2±0.6 mΩ
R_{20s}	60.7±0.7 mΩ
R_s	27.3±0.3 mΩ
R_p	19.1±0.7 mΩ
τ	1.22±0.03 ms
α	0.59±0.01

The R_p element represents the combine resistances of the SEI as well as the charge transfer (CT) resistances at anode and cathode. A change in R_p can be physically related to changing chemical composition of the electrodes such as growth of SEI/passivation layer, loss of metallic components of the cathode and/or changing crystal structure. CT resistance and SEI resistance may not change at the same rate for similar storage conditions of the battery. This could be one reason for the irregular nature of the increase in R_p seen. Increase in cathode CT resistance and decrease in anode CT resistance is seen by Stianzy et al. (experiments at high temperature 60 °C) [10]. In their results, both the SEI and cathode resistance increased substantially at 100 % SOC (much more than the minute drop in anode resistance) compared to the lower SOC case. The overall effect at high temperature and SOC is thus an increase in resistance, which is consistent with our result. The major contribution to polarization resistance, however, can be attributed to the growth of the SEI layer. The evidence of this comes from an increase in R_s which suggests that electrolyte is being lost due to reaction with lithium in forming SEI. The electrolyte is known to react with the graphite anode forming the SEI [3]. Higher voltages and temperatures, which were seen to increase the degradation rate of the electrolyte, lead to more reaction at the graphite-electrolyte interface and more SEI formation. Moreover, the SEI formed is unstable at high temperatures, leading to a continuous increase by rebuilding itself [43]. This in turn leads to a higher increase in R_p at higher SOC and higher temperatures. Röder et al. found out by studying half cells, that SEI growth is the dominant capacity fade mechanism [11]. Käbitz et al. [4] also attributed the main aging mechanism to the SEI formation on the anode.

In order to compare the two methods for calculating the resistance, the sum resistance $(R_s + R_p)$ obtained from EIS fitting is plotted along with R_{1s} obtained from the current pulses versus storage time in Fig. 5. The reason for this comparison is that the frequency just before the diffusion branch of EIS is 1 Hz for this cell (Fig. 3(a)). Thus, $(R_s + R_p)$ obtained from EIS spectra fitting corresponds to R_{1s} calculated from pulse tests. Both resistances are similar in magnitude and nature which is rather surprising as the charge transfer resistance is known to be a function of current (Butler-Volmer equation). However, the results of impedance measured at OCV and the pulse measurement at 2 C discharge pulse are similar, clearly showing that the resistance is not a strong function of current for the tested battery chemistry within the tested range of currents. This was investigated in more detail by applying pulses of different current magnitude, and determining the resistance after a duration of 1 s for a new cell at 50 % SOC. In all cases, a very low current dependency of resistance was seen (Fig. 6). The values are always found to be around 46 mΩ for a new cell.

Resistances calculated using pulses in the works of Belt et al. [20] at 30 °C, for Käbitz et al. [4] at 25 °C and 40 °C and Baghdadi et al. [22] for VL6P batteries at 30 °C and 45 °C at 30 % SOC show a fluctuating nature similar to what is observed for our low temperature data. Their high temperature data is more linear and regular, as is also seen in our case. Stiaszny et al. [10] also conducted tests at high T and high SOC storage conditions where a more linear increase with time is seen. In such cases, the average increase in R_p

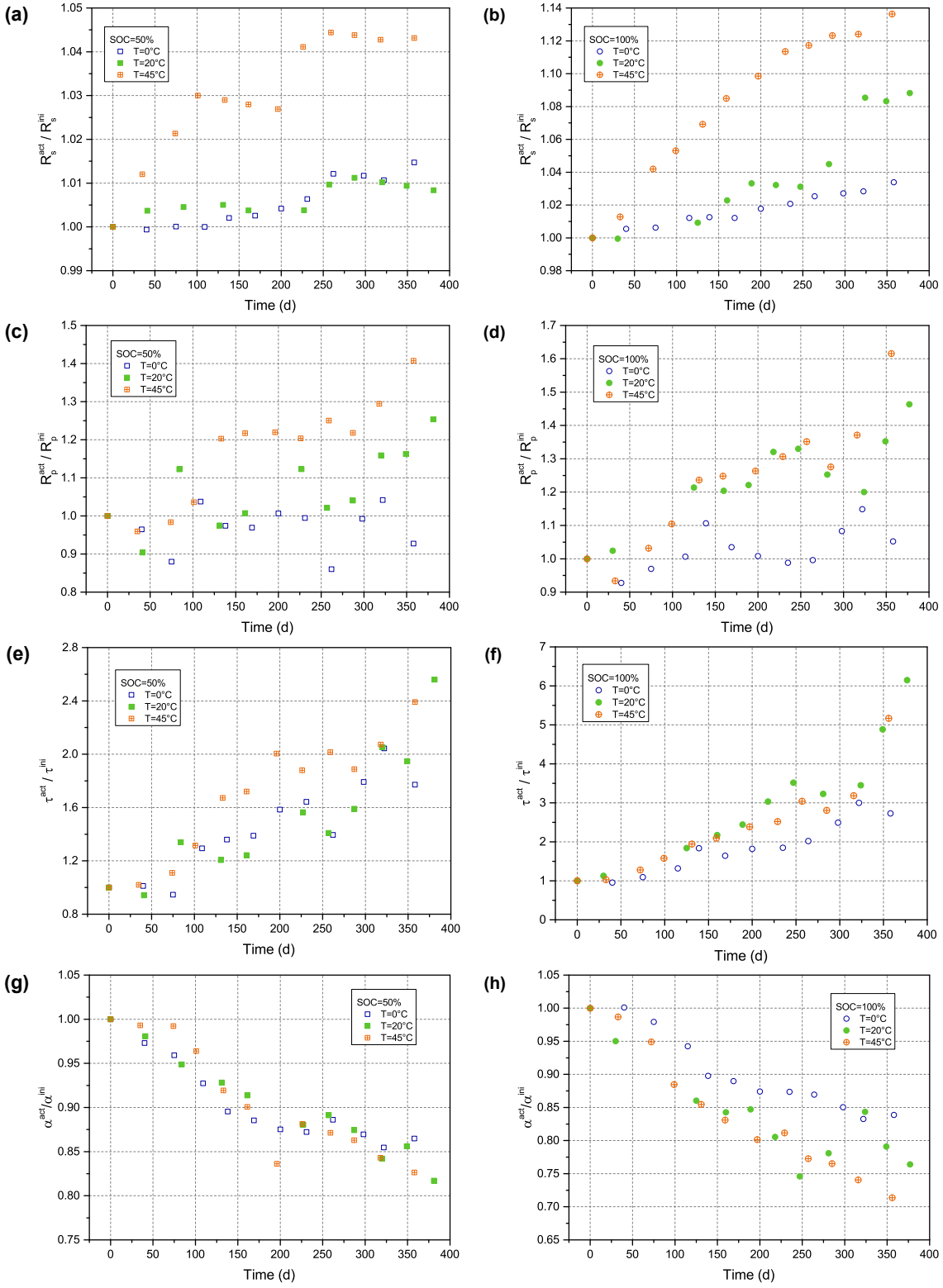

Fig. 4. Relative evolution of fitted equivalent circuit parameters with calendar aging at storage SOC of 50 % and 100 % and different storage temperatures. (a) and (b): Series resistance. (c) and (d): Parallel resistance. (e) and (f): Time constant. (g) and (h): Depression factor.

is many times compared to the increase in R_s. R_p in the case of 45 °C, 100 % SOC, is about 0.7 R_s at the initial characterization but is equal to R_s after 360 days of storage.

The mean time constant τ is interpreted as a measure of the dynamical behavior of the battery [26]. Since different surfaces on the electrode have different electrochemical activation energies, they give rise to a distribution of time constants. Hence, a mean time constant needs to be defined, while the roughness of surfaces

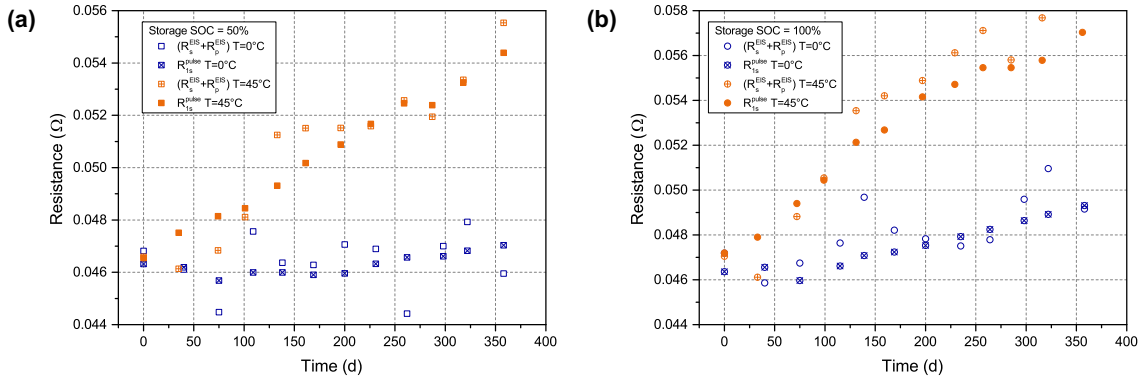

Fig. 5. Evolution of resistances during calendar aging determined via EIS ($(R_s^{EIS} + R_p^{EIS})$, around 1 Hz) and pulse test (R_{1s}^{pulse}, after 1 s pulse) at (a) 50 % storage SOC (b) 100 % storage SOC.

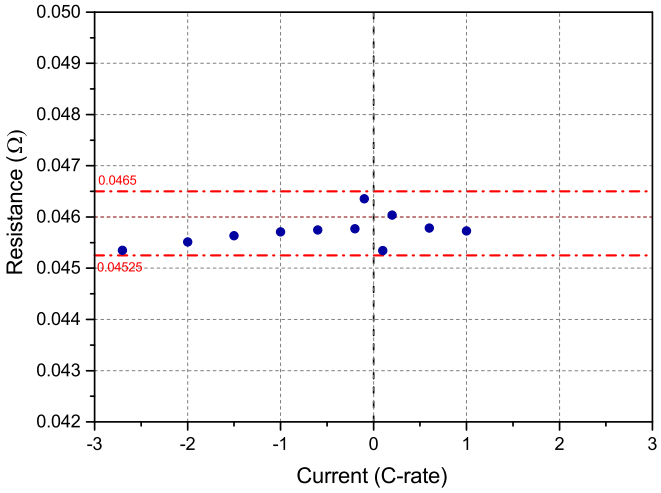

Fig. 6. Instantaneous resistance calculated at different current rates using pulse tests (horizontal lines drawn only to emphasize the low range of the resistance).

is given by α. A higher time constant signifies a slower response of the battery to the current pulse. Hence, the voltage change due to a current pulse is slower in case of a higher time constant. The increase in time constant is found to be a strong function of SOC and has a weak temperature dependence, as can be seen from Fig. 4(e) and (f). The nature of increase of time constant is exponential with storage time. An increase in time constant is seen also in the experimental results of Waag et al. [26] through the Nyquist plots of new and aged cells looking at the values of the critical frequencies at the intercept of the real axis, the maximum of the depressed semicircle and the starting point of the diffusion branch.

The depression factor α is the measure of depression of the semicircle given by the ZARC element, which arises due to the porous micro-structure of the electrodes and as such it is a measure of the non-uniformity of the electrode surfaces [37]. In all cases of temperature and SOC, a decrease in α is seen with storage time (Fig. 4(g) and (h)). Change in α is dependent on storage SOC with greater decrease at 100 % SOC than at 50 % SOC. Also, a stronger temperature dependency is noticed at 100 % SOC than at 50 % SOC. Decreasing α represents greater depression of the semicircle, which in turn could represent an increasing non-uniformity of electrode surfaces probably due to an increasing porosity. Particle fracture, which can cause an increase of porosity in the NMC particles, was observed by Stiaszny et al. [10]. This was more prominently seen at high voltage (or high SOC), consistent with our results. A decrease of α, pointing to an increase of active surface area, could also affect the charge transfer resistance by decreasing it, as noticed in the case of graphite anode by Stianzy et al. [10].

A word of caution here, the decrease in α should be interpreted carefully given the fact that the SEI and the CT semicircles separate with aging as the CT semicircle moves towards lower frequencies (seen by increase in τ, also Fig. 3(a)). The two (or more) separated processes, when fit by only one ZARC element, can lead to an exaggerated apparent decrease in the value of α.

3.3. Influence of electrochemical characterization

3.3.1. Reference cells

Four cells were characterized initially and after 186 days of storage at 20 °C, but not intermediately unlike the other cells. These cells are referred to as reference cells. Their relative capacity fade is displayed in Fig. 1 along with the capacity fade of the cells that were characterized every 30 days. The reference cells are used to study the influence of the regular characterization procedures on cell degradation. It is seen that the capacity fade after 186 days is significantly smaller for the reference cells compared to the cells stored at the same conditions that where characterized every 30 days. The capacity loss of the reference cells follows the same SOC dependency as the other cells.

A significant difference between regularly characterized cells and reference cells can also be observed for the change of internal resistance with time as depicted in Fig. 2. R_{1s} only increases by about 2 % after 186 days for the reference cell stored at 100 % SOC, while R_{1s} of the regular cells stored at this SOC increases by about 7 % during the same time. The other reference cells even show a decrease in R_{1s} after 186 days. The same nature is observed for R_{20s}.

The faster aging of the regular characterized cells can be explained by additional degradation due to the electrochemical characterization, which induces charging and discharging of the cells. It is commonly accepted that cycling lithium-ion cells leads to enhanced degradation compared to calendar aging [9,21]. Additional mechanical degradation resulting from volume changes of the graphite anode during charging and discharging [44], can lead to cracking of the SEI. The subsequent repair resulting in additional lithium consumption and therefore capacity loss [15].

Even while this experiment needs to be repeated with a larger number of samples, this is already a strong hint that the electrochemical characterization during calendar aging tests has a non-negligible impact on the measured capacity fade and inner resistance change.

3.3.2. Influence of differences in resetting the SOC

The charge throughput experienced by a cell during to characterizations and resetting of SOC (see section 2) can be quantified in equivalent full cycles (EFC). One EFC corresponds to two times the rated capacity (1 EFC = 4.3 Ah). During the test period the cells stored at 50 % SOC and 100 % SOC and 20 °C experienced approximately 60 equivalent full cycles due to the characterizations and resetting of SOC. The cells stored at 25 % SOC and 75 % SOC 20 °C experienced approximately 100 and 92 equivalent full cycles during the same time period, i.e. these cells have 50 % more charge throughout than the cells stored at 50, 100 % SOC. This is due to the procedures that were used in this study to set different SOC levels after characterization and offers another possibility to analyze the influence of charge throughput on the measured aging. In Fig. 7(a) the residual cell capacity is plotted as a function of charge throughput Q instead of time as in Fig. 1. As discussed in section 3.1, the cells stored at 25 % SOC and 75 % SOC show an unexpected fast capacity fade compared to the cells stored at 50 % SOC and 100 % SOC when capacity fade is regarded as a function of time. But when capacity fade is regarded as a function of charge throughput, the cells stored at 25 % SOC show the slowest rate of capacity decrease followed by the cells stored at 50 % SOC which is as expected. It can thus be inferred that the relatively high rate of capacity fade of the cells stored at 25 % SOC when compared to cells stored at 50 % SOC is due to the additional cycling these cells experienced during resetting of the SOC.

This can also be assumed for the cells stored at 75 % SOC, which exhibit the fastest capacity decrease as a function of time, as seen from Fig. 1(a). When plotted against charge throughput, the cells stored at 75 % SOC show a similar rate of capacity fade as the cells stored at 100 % SOC, as depicted in Fig. 7(a).

In Fig. 7(b), the change of internal resistance R_{20s} is plotted as a function of charge throughput. The resistance of the cells stored at 50 % still rises the slowest but the difference to the cells stored at 25 % is much smaller than in the case of using time as independent variable.

The internal resistance of the reference cells does not rise significantly faster than the internal resistance of the cells which were characterized regularly as shown in Fig. 7(b). This suggests that the rise of internal resistance during calendar aging actually might be mainly due to the cycling during characterizations.

3.3.3. Influence seen through EIS analysis

Additional proof that characterization affects calendar aging comes from EIS analysis. In Fig. 4 greater increase in R_s, R_p and τ as well as greater decrease in α is seen for the 100 % SOC case compared to 50 % SOC. This is as expected, as greater SOC or greater voltage is known to enhance calender aging [8,12].

However, looking at the parameters R_s and τ for cells also stored at 25 % SOC and 75 % SOC at 20 °C in Fig. 8, it can be clearly seen that 50 % SOC has the least increase of R_s and τ.

Considering this anomaly in light of the characterization procedure used, it is clear that the additional degradation seen at 25 % SOC is due to the characterization. The cells stored at 25 % SOC and 75 % SOC experience more charge throughput than the cells stored at 50 % SOC and 100 % SOC. The additional aging due to increased characterizations in the case of 75 % SOC are probably masked by the much greater increase in calendar aging of 100 % SOC cells [8,12]. In fact, if the data from 50 % SOC is ignored, the 25 %, 75 % and 100 % SOC line up as expected for all four parameters (Fig. 8).

3.3.4. Consequences for lifetime predictions

As stated before, forecasts on the expected battery lifetime under given operating conditions is a main aim of aging studies. It is usually assumed that a battery has reached its end of life (EOL) when its actual capacity has dropped to 80 % of its initial value. The expected calendar lifetime t_{EOL} based on the linear aging model (Eq. (2)) parametrized in section 3.1 is listed in Table 5.

The impact of calendar aging on cycle aging tests has been discussed in the literature [21,45]. In contrast to that, the effect of electrochemical characterizations on calendar aging tests has mostly been neglected so far. The linear aging model (Eq. (2)) can be parametrized based on the experimental data obtained from the capacity fade of the reference cells in order to estimate the influence of the characterization method on lifetime predictions. The resulting aging factor $b_{2\,ref}$ and the corresponding expected calendar lifetime $t_{EOL\,ref}$ are presented in Table 5.

For all storage conditions except 75 % SOC, the expected calendar lifetime is at least 50 % longer when the reference cells are used for parameterizing the aging model. The common procedure of alternating storing and characterizing lithium-ion cells [4,8,9,21,22] might thus lead to an overestimation of calendar aging as the measured capacity decrease is not solely due to calendar aging but also includes the cycle aging caused by the characterizations.

It is also possible that the apparent linearity of the capacity fade with storage time observed in this study is caused by the regular characterizations, as capacity fade during cycle aging has been reported to be linear with charge throughput, at least in the early stage of a battery's lifetime [1,46,47].

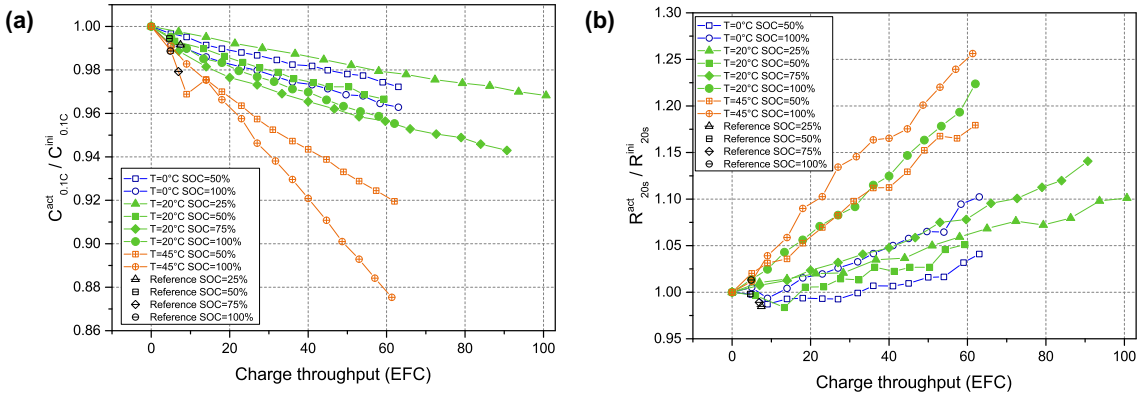

Fig. 7. Change of cell parameters plotted versus charge throughput in equivalent full cycles (EFC). Results from calendar aging tests and reference cells, which were stored for 186 days at 20 °C with no intermediate characterizations, are shown. (a) Relative cell capacity measured at 0.1 C discharging. (b) Relative internal resistance determined from 2 C discharging pulses.

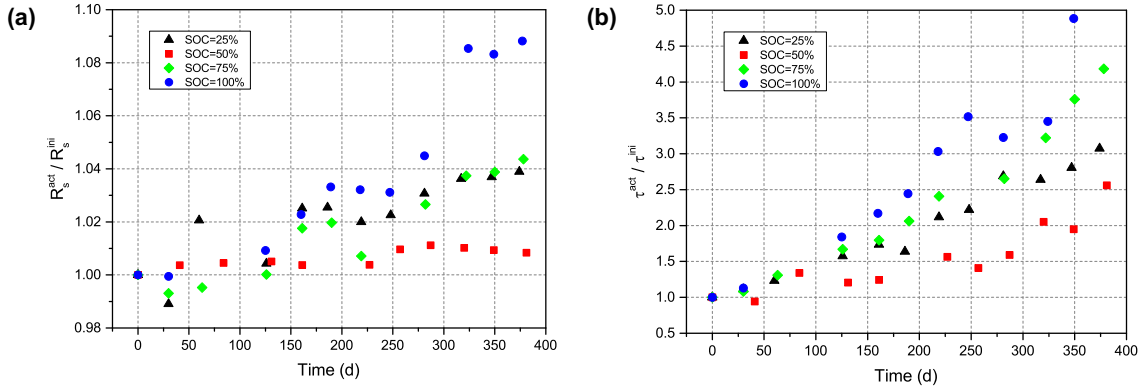

Fig. 8. Fitted equivalent circuit parameters from EIS analysis of batteries calendar aged at 20 °C at different SOC plotted versus storage time. (a) Serial resistance and (b) time constant of the ZARC element.

Table 5
Linear aging factor $b_{2\ ref}$ and predicted calendar lifetime $t_{EOL\ ref}$ for reference cells stored at 20 °C with no intermediate characterizations and predicted calendar lifetime based on calendar aging tests with regular characterizations t_{EOL}.

SOC (%)	$b_{2\ ref}$ (d^{-1})	$t_{EOL\ ref}$ (y)	t_{EOL} (y)
25	4.56E-05	12.0	7.9
50	2.98E-05	18.4	8.0
75	1.12E-04	4.9	4.8
100	6.08E-05	9.0	6.0

4. Conclusion

In this work, the capacity fade and impedance rise of commercial 18650 lithium-ion batteries due to calendar aging were studied. The capacity of the studied cells is found to decrease in a linear way with storage time. The rate of capacity fade is higher at higher temperatures during storage. The internal resistance of cells, based on current pulse measurements, is found to increases with storage time. Interestingly, the internal resistance calculated from the voltage drop after 1 s of current pulse and the internal resistance based on the voltage drop after 20 s of current pulse always have the same ratio of about 76 % for all aging stages and under all aging conditions. This means that the aging affects fast processes (ohmic resistance, polarization resistance) and slower processes (diffusion) in a similar way.

EIS spectra were fit by an equivalent circuit model representing ohmic resistance, polarization resistance, capacitive effects and diffusion processes in order to quantify changes of these parameters with aging. The ohmic and the polarization resistance were found to increase with storage time with the increase of polarization resistance being much larger. The time constant of the polarization and the depression of the polarization semi-circle was found to increase with storage time. The values for the internal resistance determined after 1 s pulses are in good agreement with the sum of ohmic and polarization resistance from the EIS analysis signifying low current dependency of polarization resistance.

It was observed that the results of the calendar aging study are significantly influenced by the characterizations and the resetting of SOC. This has so far mostly been neglected in the literature where similar storage periods between electrochemical characterizations and similar procedures of electrochemical characterization are seen. It can be assumed that the influence of aging processes occurring during storage is often overestimated and the real battery lifetime without any operation is longer than inferred from calendar aging studies which include frequent electrochemical characterizations. Further experiments that quantitatively investigate the impact of the electrochemical characterization need to be conducted and the influence should be considered during the design and analysis of future calendar aging studies. Such information can also help select the periodicity of the electrochemical characterizations to ensure minimum influence on calendar aging from them. One way to quantify the aging due to charge throughput is to study cycle aging. The authors plan to present an analysis of the cycle aging behavior of the tested cells in a separate publication.

Acknowledgments

This work was funded as part of the project "Materials for Ageing Resistant Li-ion High Energy Storage for Electric Vehicles" (MARS-EV, EC FP7 Grant Agreement no. 609201). Additionally, Arpit Maheshwari would like to acknowledge Erasmus Mundus Joint Doctoral Programme SELECT+ and KIC InnoEnergy Phd School for funding his doctoral studies.

References

[1] R. Spotnitz, Simulation of capacity fade in lithium-ion batteries, J. Power Sources 113 (1) (2003) 72–80, http://dx.doi.org/10.1016/S0378-7753(02)00490-1.
[2] H.J. Ploehn, P. Ramadass, R.E. White, Solvent diffusion model for aging of lithium-ion battery cells, J. Electrochem. Soc. 151 (3) (2004) A456–A462, http://dx.doi.org/10.1149/1.1644601.
[3] M. Broussely, P. Biensan, F. Bonhomme, P. Blanchard, S. Herreyre, K. Nechev, R.J. Staniewicz, Main aging mechanisms in Li ion batteries, J. Power Sources 146 (1–2) (2005) 90–96, http://dx.doi.org/10.1016/j.jpowsour.2005.03.172.
[4] S. Käbitz, J.B. Gerschler, M. Ecker, Y. Yurdagel, B. Emmermacher, D. André, T. Mitsch, D.U. Sauer, Cycle and calendar life study of a graphite—LiNi1/3Mn1/3Co1/3O2 Li-ion high energy system. Part A: full cell characterization, J. Power Sources 239 (2013) 572–583, http://dx.doi.org/10.1016/j.jpowsour.2013.03.045.
[5] J. Wang, J. Purewal, P. Liu, J. Hicks-Garner, S. Soukazian, E. Sherman, A. Sorenson, L. Vu, H. Tataria, M.W. Verbrugge, Degradation of lithium ion batteries employing graphite negatives and nickel–cobalt–manganese oxide + spinel manganese oxide positives: Part 1, aging mechanisms and life estimation, J. Power Sources 269 (2014) 937–948, http://dx.doi.org/10.1016/j.jpowsour.2014.07.030.
[6] K. Jalkanen, J. Karppinen, L. Skogström, T. Laurila, M. Nisula, K. Vuorilehto, Cycle aging of commercial NMC/graphite pouch cells at different temperatures, Appl. Energy 154 (2015) 160–172, http://dx.doi.org/10.1016/j.apenergy.2015.04.110.
[7] D. Li, D.L. Danilov, J. Xie, L. Raijmakers, L. Gao, Y. Yang, P.H. Notten, Degradation mechanisms of C6/LiFePO4 batteries: experimental analyses of calendar aging, Electrochim. Acta 190 (2016) 1124–1133, http://dx.doi.org/10.1016/j.electacta.2015.12.161.
[8] P. Keil, S.F. Schuster, J. Wilhelm, J. Travi, A. Hauser, R.C. Karl, A. Jossen, Calendar aging of lithium-ion batteries, J. Electrochem. Soc. 163 (9) (2016) A1872–A1880, http://dx.doi.org/10.1149/2.0411609jes.
[9] M. Ecker, J.B. Gerschler, J. Vogel, S. Käbitz, F. Hust, P. Dechent, D.U. Sauer, Development of a lifetime prediction model for lithium-ion batteries based on extended accelerated aging test data, J. Power Sources 215 (2012) 248–257, http://dx.doi.org/10.1016/j.jpowsour.2012.05.012.

[10] B. Stiaszny, J.C. Ziegler, E.E. Krauß, M. Zhang, J.P. Schmidt, E. Ivers-Tiffée, Electrochemical characterization and post-mortem analysis of aged LiMn2O4–NMC/graphite lithium ion batteries part II: calendar aging, J. Power Sources 258 (2014) 61–75, http://dx.doi.org/10.1016/j.jpowsour.2014.02.019.
[11] P. Röder, B. Stiaszny, J.C. Ziegler, N. Baba, P. Lagaly, H.-D. Wiemhöfer, The impact of calendar aging on the thermal stability of a LiMn2o4–Li(Ni1/3mn1/3co1/3)O2/graphite lithium-ion cell, J. Power Sources 268 (2014) 315–325, http://dx.doi.org/10.1016/j.jpowsour.2014.06.040.
[12] M. Ecker, N. Nieto, S. Käbitz, J. Schmalstieg, H. Blanke, A. Warnecke, D.U. Sauer, Calendar and cycle life study of Li(NiMnCo)O2-based 18650 lithium-ion batteries, J. Power Sources 248 (2014) 839–851, http://dx.doi.org/10.1016/j.jpowsour.2013.09.143.
[13] P. Liu, J. Wang, J. Hicks-Garner, E. Sherman, S. Soukiazian, M. Verbrugge, H. Tataria, J. Musser, P. Finamore, Aging mechanisms of LiFePO4 batteries deduced by electrochemical and structural analyses, J. Electrochem. Soc. 157 (4) (2010) A499–A507, http://dx.doi.org/10.1149/1.3294790.
[14] M. Safari, C. Delacourt, Aging of a commercial graphite/LiFePO4 cell, J. Electrochem. Soc. 158 (10) (2011) A1123–A1135, http://dx.doi.org/10.1149/1.3614529.
[15] E. Peled, The electrochemical behavior of alkali and alkain earth Metals in nonaqueous battery systems - the solid electrolyte interphase model, J. Electrochem. Soc. 126 (12) (1979) 2047–2051.
[16] J. Christensen, J. Newman, A Mathematical model for the lithium-ion negative electrode solid electrolyte interphase, J. Electrochem. Soc. 151 (11) (2004) A1977–A1988, http://dx.doi.org/10.1149/1.1804812.
[17] I. Buchberger, S. Seidlmayer, A. Pokharel, M. Piana, J. Hattendorff, P. Kudejova, R. Gilles, H.A. Gasteiger, Aging analysis of graphite/LiNi1/3Mn1/3Co1/3O2 cells using XRD, PGAA, and AC impedance, J. Electrochem. Soc. 162 (14) (2015) A2737–A2746, http://dx.doi.org/10.1149/2.0721514jes.
[18] D. Li, D. Danilov, Z. Zhang, H. Chen, Y. Yang, P.H.L. Notten, Modeling the SEI-formation on graphite electrodes in LiFePO4 batteries, J. Electrochem. Soc. 162 (6) (2015) A858–A869, http://dx.doi.org/10.1149/2.0161506jes.
[19] J. Wang, P. Liu, J. Hicks-Garner, E. Sherman, S. Soukiazian, M. Verbrugge, H. Tataria, J. Musser, P. Finamore, Cycle-life model for graphite-LiFePO4 cells, J. Power Sources 196 (8) (2011) 3942–3948, http://dx.doi.org/10.1016/j.jpowsour.2010.11.134.
[20] J. Belt, V. Utgikar, I. Bloom, Calendar and PHEV cycle life aging of high-energy, lithium-ion cells containing blended spinel and layered-oxide cathodes, J. Power Sources 196 (23) (2011) 10213–10221, http://dx.doi.org/10.1016/j.jpowsour.2011.08.067.
[21] J. Schmalstieg, S. Käbitz, M. Ecker, D.U. Sauer, A holistic aging model for Li(NiMnCo)O2 based 18650 lithium-ion batteries, J. Power Sources 257 (2014) 325–334, http://dx.doi.org/10.1016/j.jpowsour.2014.02.012.
[22] I. Baghdadi, O. Briat, J.-Y. Delétage, P. Gyan, J.-M. Vinassa, Lithium battery aging model based on Dakin's degradation approach, J. Power Sources 325 (2016) 273–285, http://dx.doi.org/10.1016/j.jpowsour.2016.06.036.
[23] R.G. Jungst, G. Nagasubramanian, H.L. Case, B.Y. Liaw, A. Urbina, T.L. Paez, D.H. Doughty, Accelerated calendar and pulse life analysis of lithium-ion cells, J. Power Sources 119–121 (2003) 870–873, http://dx.doi.org/10.1016/S0378-7753(03)00193-9.
[24] S. Buller, Impedance based simulation models for energy storage devices in advanced automotive power systems, Vol. 31 of Aachener Beiträge des ISEA, Shaker, Aachen, 2003.
[25] D. Andre, M. Meiler, K. Steiner, H. Walz, T. Soczka-Guth, D.U. Sauer, Characterization of high-power lithium-ion batteries by electrochemical impedance spectroscopy, II Model. J. Power Sources 196 (12) (2011) 5349–5356, http://dx.doi.org/10.1016/j.jpowsour.2010.07.071.
[26] W. Waag, S. Käbitz, D.U. Sauer, Experimental investigation of the lithium-ion battery impedance characteristic at various conditions and aging states and its influence on the application, Appl. Energy 102 (2013) 885–897, http://dx.doi.org/10.1016/j.apenergy.2012.09.030.
[27] A. Eddahech, O. Briat, J.-M. Vinassa, Determination of lithium-ion battery state-of-health based on constant-voltage charge phase, J. Power Sources 258 (2014) 218–227, http://dx.doi.org/10.1016/j.jpowsour.2014.02.020.
[28] M. Abdel Monem, K. Trad, N. Omar, O. Hegazy, B. Mantels, G. Mulder, P. van den Bossche, J. van Mierlo, Lithium-ion batteries: evaluation study of different charging methodologies based on aging process, Appl. Energy 152 (2015) 143–155, http://dx.doi.org/10.1016/j.apenergy.2015.02.064.
[29] M.-S. Wu, P.-C.J. Chiang, J.-C. Lin, Electrochemical investigations on advanced lithium-ion batteries by three-electrode measurements, J. Electrochem. Soc. 152 (1) (2005) A47, http://dx.doi.org/10.1149/1.1825385.
[30] U. Tröltzsch, O. Kanoun, H.-R. Tränkler, Characterizing aging effects of lithium ion batteries by impedance spectroscopy, Electrochim. Acta 51 (8–9) (2006) 1664–1672, http://dx.doi.org/10.1016/j.electacta.2005.02.148.
[31] L. Lavigne, J. Sabatier, J.M. Francisco, F. Guillemard, A. Noury, Lithium-ion Open Circuit Voltage (OCV) curve modelling and its ageing adjustment, J. Power Sources 324 (2016) 694–703, http://dx.doi.org/10.1016/j.jpowsour.2016.05.121.
[32] J.P. Schmidt, H.Y. Tran, J. Richter, E. Ivers-Tiffée, M. Wohlfahrt-Mehrens, Analysis and prediction of the open circuit potential of lithium-ion cells, J. Power Sources 239 (2013) 696–704, http://dx.doi.org/10.1016/j.jpowsour.2012.11.101.
[33] M. Broussely, S. Herreyre, P. Biensan, P. Kasztejna, K. Nechev, R. Staniewicz, Aging mechanism in Li ion cells and calendar life predictions, J. Power Sources 97–98 (2001) 13–21, http://dx.doi.org/10.1016/S0378-7753(01)00722-4.
[34] E. Barsoukov, J.R. MacDonald, Impedance Spectroscopy: Theory, Experiment, and Applications, John Wiley & Sons, Hoboken, N.J, 2005.
[35] H. Andersson, I. Petersson, E. Ahlberg, Modelling electrochemical impedance data for semi-bipolar lead acid batteries, J. Appl. Electrochem 31 (1) (2001) 1–11, http://dx.doi.org/10.1023/A:1004105622558.
[36] F. La Mantia, Characterization of Electrodes for Lithium-ion Batteries through Electrochemical Impedance Spectroscopy and Mass Spectrometry, Ph.D. Thesis, ETH Zürich, 2008.
[37] J.-B. Jorcin, M.E. Orazem, N. Pébère, B. Tribollet, CPE analysis by local electrochemical impedance spectroscopy, Electrochim. Acta 51 (8–9) (2006) 1473–1479, http://dx.doi.org/10.1016/j.electacta.2005.02.128.
[38] B. Stiaszny, J.C. Ziegler, E.E. Krauß, J.P. Schmidt, E. Ivers-Tiffée, Electrochemical characterization and post-mortem analysis of aged LiMn2o4–Li(Ni0.5mn0.3co0.2)O2/graphite lithium ion batteries. Part I: cycle aging, J. Power Sources 251 (2014) 439–450, http://dx.doi.org/10.1016/j.jpowsour.2013.11.080. URL, https://www.sciencedirect.com/science/article/pii/S0378775313019150.
[39] J. Bisquert, G. Garcia-Belmonte, P. Bueno, E. Longo, L. Bulhões, Impedance of constant phase element (CPE)-blocked diffusion in film electrodes, J. Electroanal. Chem. 452 (2) (1998) 229–234, http://dx.doi.org/10.1016/S0022-0728(98)00115-6.
[40] J. Song, M.Z. Bazant, Effects of nanoparticle geometry and size distribution on diffusion impedance of battery electrodes, J. Electrochem. Soc. 160 (1) (2012) A15–A24, http://dx.doi.org/10.1149/2.023301jes.
[41] J.W. Eaton, D. Bateman, S. Hauberg, R. Wehbring, GNU Octave Version 4.0.0 Manual: a High-level Interactive Language for Numerical Computations, 2015. URL, http://www.gnu.org/software/octave/doc/interpreter.
[42] J. Vetter, P. Novák, M.R. Wagner, C. Veit, K.C. Möller, J.O. Besenhard, M. Winter, M. Wohlfahrt-Mehrens, C. Vogler, A. Hammouche, Ageing mechanisms in lithium-ion batteries, J. Power Sources 147 (1–2) (2005) 269–281, http://dx.doi.org/10.1016/j.jpowsour.2005.01.006.
[43] Y. Zheng, M. Ouyang, L. Lu, J. Li, Understanding aging mechanisms in lithium-ion battery packs: from cell capacity loss to pack capacity evolution, J. Power Sources 278 (2015) 287–295, http://dx.doi.org/10.1016/j.jpowsour.2014.12.105.
[44] R.S. Rubino, H. Gan, E.S. Takeuchi, A study of capacity fade in cylindrical and prismatic lithium-ion batteries, J. Electrochem. Soc. 148 (9) (2001) A1029–A1033, http://dx.doi.org/10.1149/1.1390344.
[45] A.J. Smith, H.M. Dahn, J.C. Burns, J.R. Dahn, Long-term low-rate cycling of LiCoO2/graphite Li-Ion cells at 55°C, J. Electrochem. Soc. 159 (6) (2012) A705–A710, http://dx.doi.org/10.1149/2.056206jes.
[46] K. Takei, K. Kumai, Y. Kobayashi, H. Miyashiro, N. Terada, T. Iwahori, T. Tanaka, Cycle life estimation of lithium secondary battery by extrapolation method and accelerated aging test, J. Power Sources 97–98 (2001) 697–701, http://dx.doi.org/10.1016/S0378-7753(01)00646-2.
[47] T. Waldmann, M. Wilka, M. Kasper, M. Fleischhammer, M. Wohlfahrt-Mehrens, Temperature dependent ageing mechanisms in Lithium-ion batteries – a Post-Mortem study, J. Power Sources 262 (2014) 129–135, http://dx.doi.org/10.1016/j.jpowsour.2014.03.112.